Supplementary Materials for

How Particle–Particle and Liquid–Particle Interactions Govern the Fate of Evaporating Liquid Marbles

Adair Gallo Jr.*, **Fernanda Tavares, Ratul Das, Himanshu Mishra***

*Corresponding author. Email: Himanshu.Mishra@Kaust.edu.sa; Adair.GalloJunior@Kaust.edu.sa

This PDF file includes:

Supplementary Text
Figs. S1 to S11
Captions for Movies S1 to S2

Other Supplementary Materials for this manuscript include the following:

Movies S1 to S2

Supplementary Text

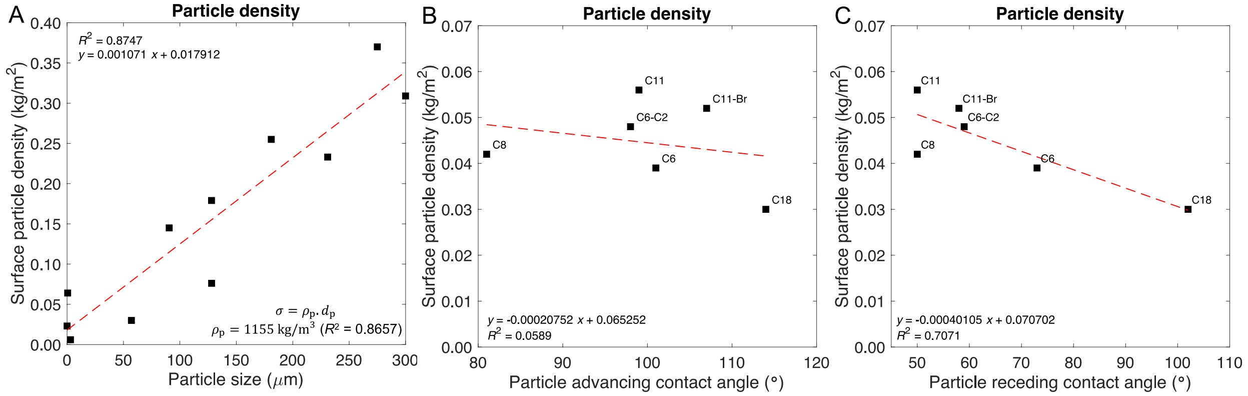

Fig. S1.

Marble surface particle density, σ, and correlations for 10-µL water marbles. (A) Effects of varying particle sizes with constant chemical composition (C18). **(B)** Effects of varying chemical compositions of particles at a fixed particle size of 57 µm. Note: particle-level increasing and **(C)** decreasing contact angles of water droplets were obtained via the silanization of flat silica surfaces with the specified functional groups (e.g., C8, C11, etc.).

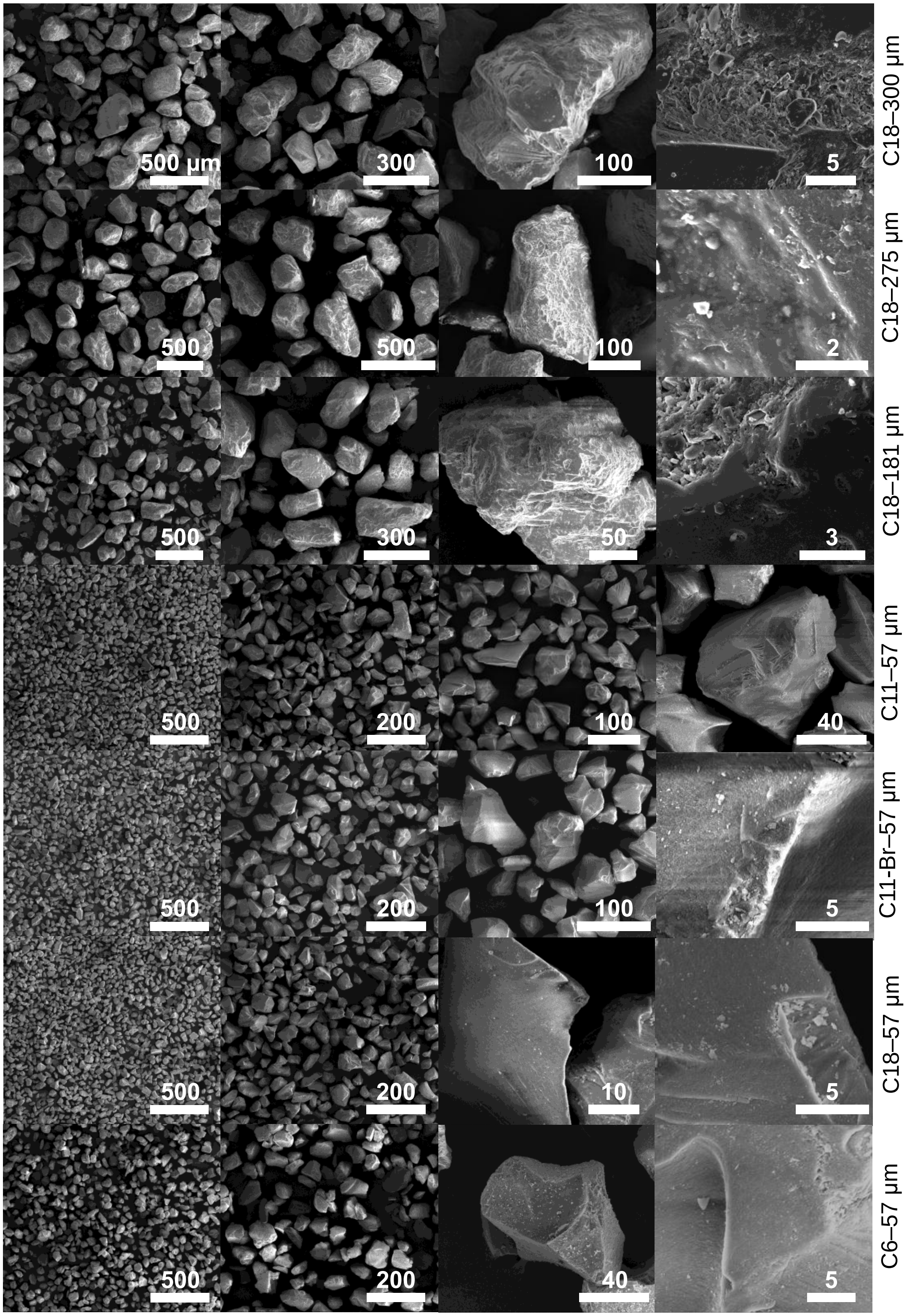

Fig. S2.

Scanning electron micrographs of sand and silica particles used to fabricate the liquid marbles. Scale bars are in micrometers.

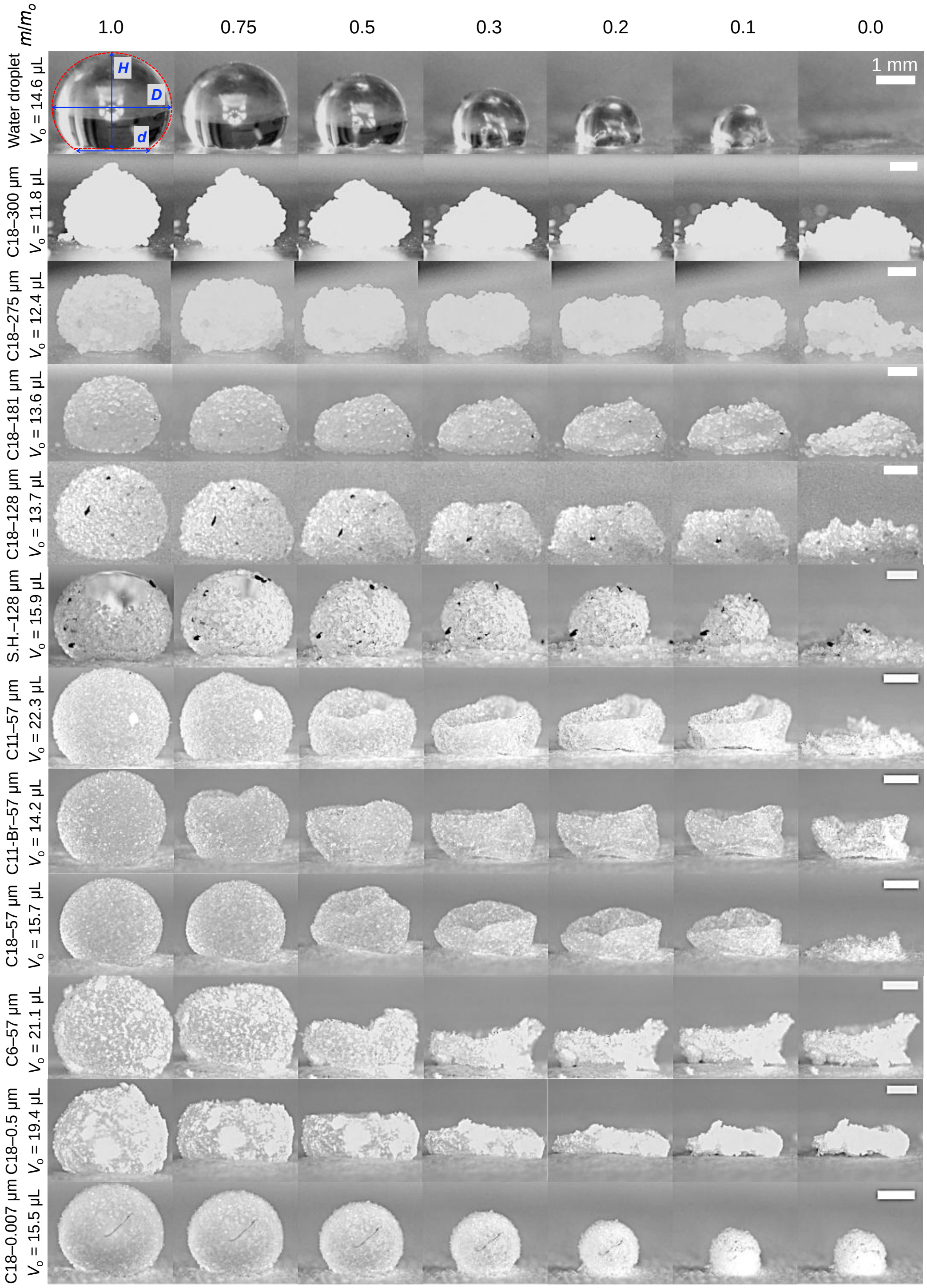

Fig. S3.

Time-lapse photographs of the evaporation of (topmost) water droplets on a hydrophobic glass slide (H-glass) and of several water marbles coated with C18; the particle sizes vary from 0.007 to 300 µm.

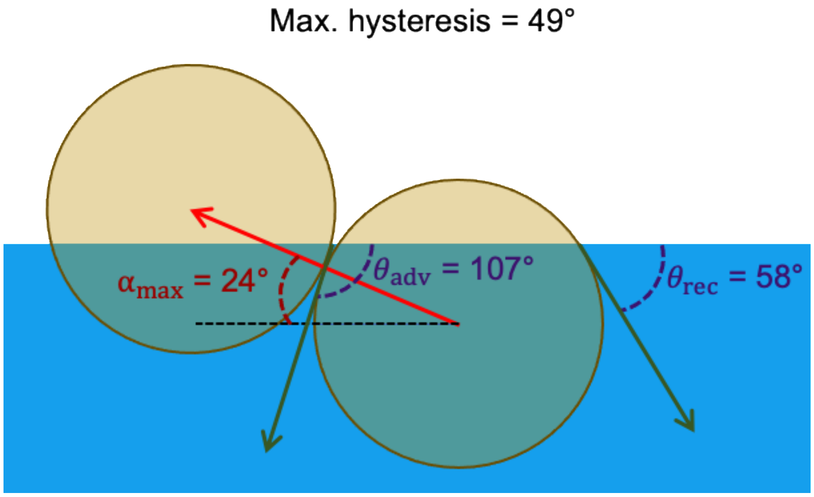

Fig. S4.

Estimation of the maximum particle misalignment, $\alpha_{\max} = 24°$, for the maximum value of contact angle hysteresis for the experimental particles we studied (Table 1). This analysis assumes that the particles are spherical and smooth and that there is no lateral compression force, i.e., the particles are at equilibrium at $m/m_o = 1$.

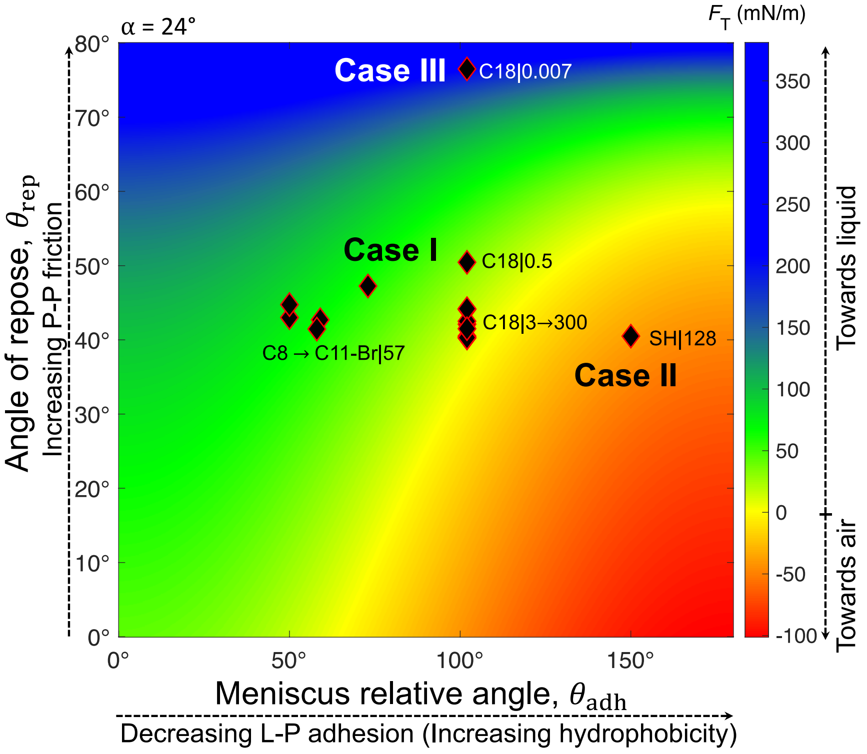

Fig. S5.

Analytic framework diagram for the maximum estimated particle misalignment at equilibrium contact angles $\alpha_{\max} = 24°$, with overlaying experimental points from Table 1.

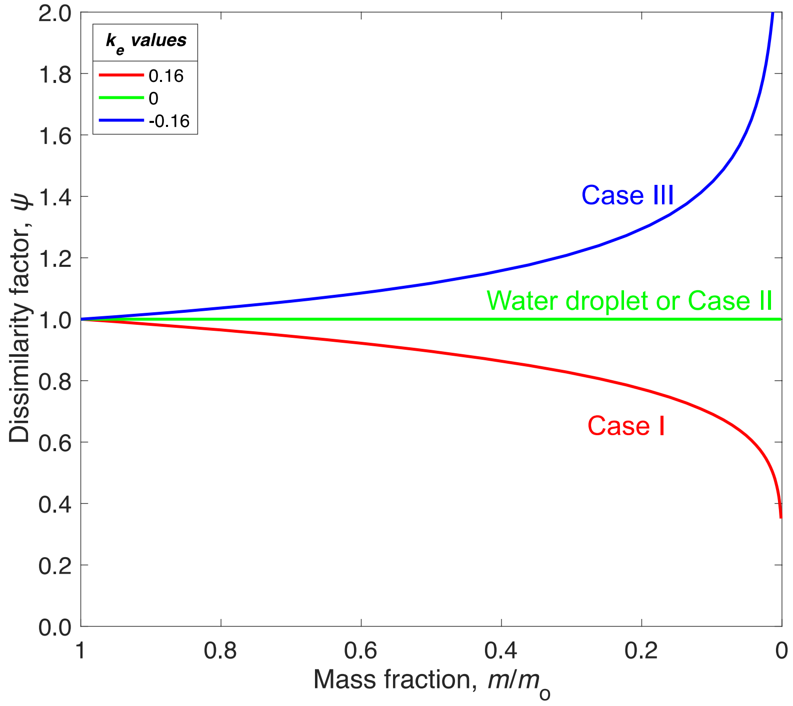

Fig. S6.

Dependence of the dissimilarity factor, ψ, on the liquid mass fraction for three typical k_e values.

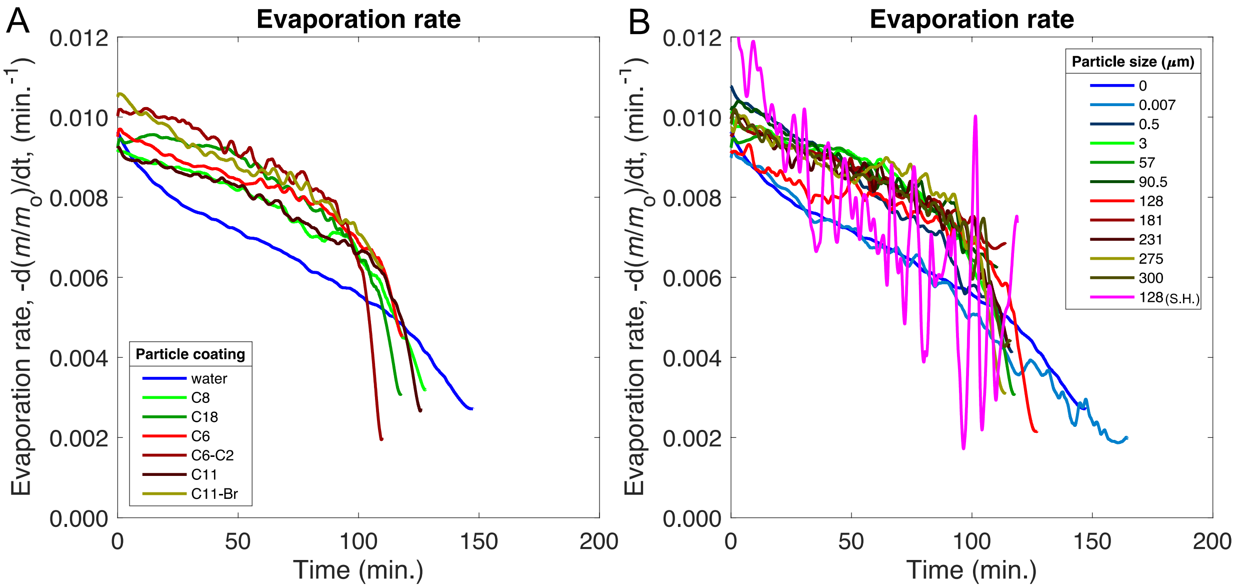

Fig. S7.

Variation in the evaporation rates of liquid marbles over time. (A) Effects of chemical compositions at a fixed particle size of 57 µm; **(B)** effects of particle size with a fixed chemical composition of C18 (ODTS). Note: The volume of water inside the marbles was 10 µL, and evaporation experiments were performed at 23 ± 1°C and 60 ± 2% relative humidity (RH).

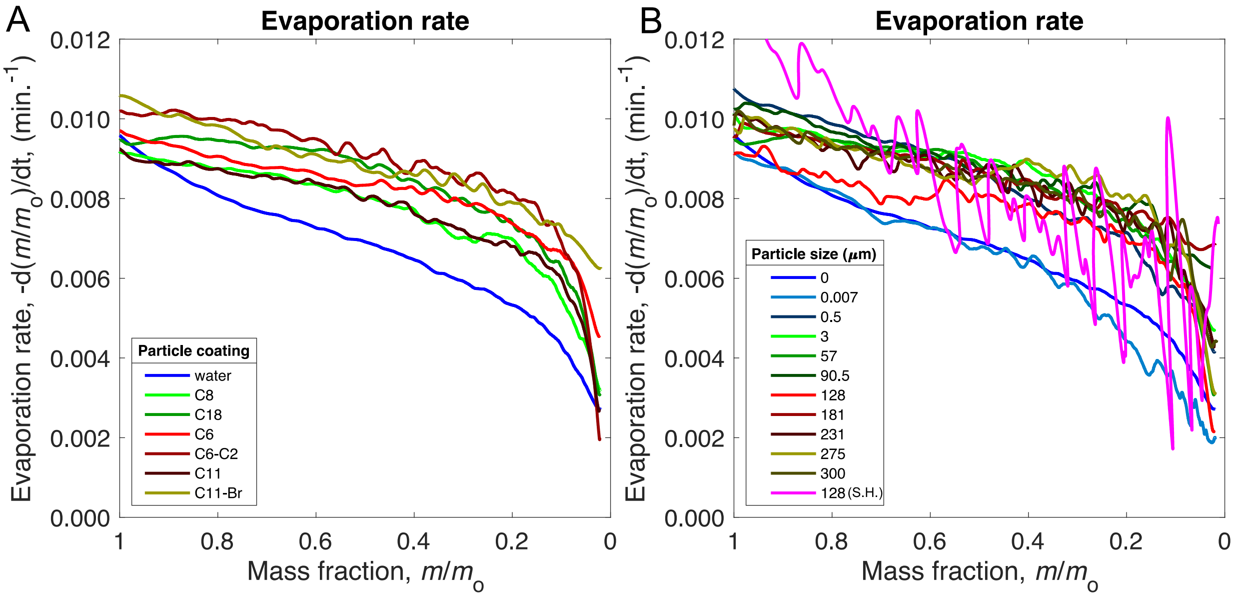

Fig. S8.

Variation in the evaporation rates as a function of mass fraction. (A) Effects of chemical compositions at a fixed particle size fixed of 57 µm; **(B)** effects of particle size with a fixed chemical composition of C18 (ODTS). Note: The volume of water inside the marbles was 10 µL, and the evaporation experiments were performed at 23 ± 1°C and 60 ± 2% RH.

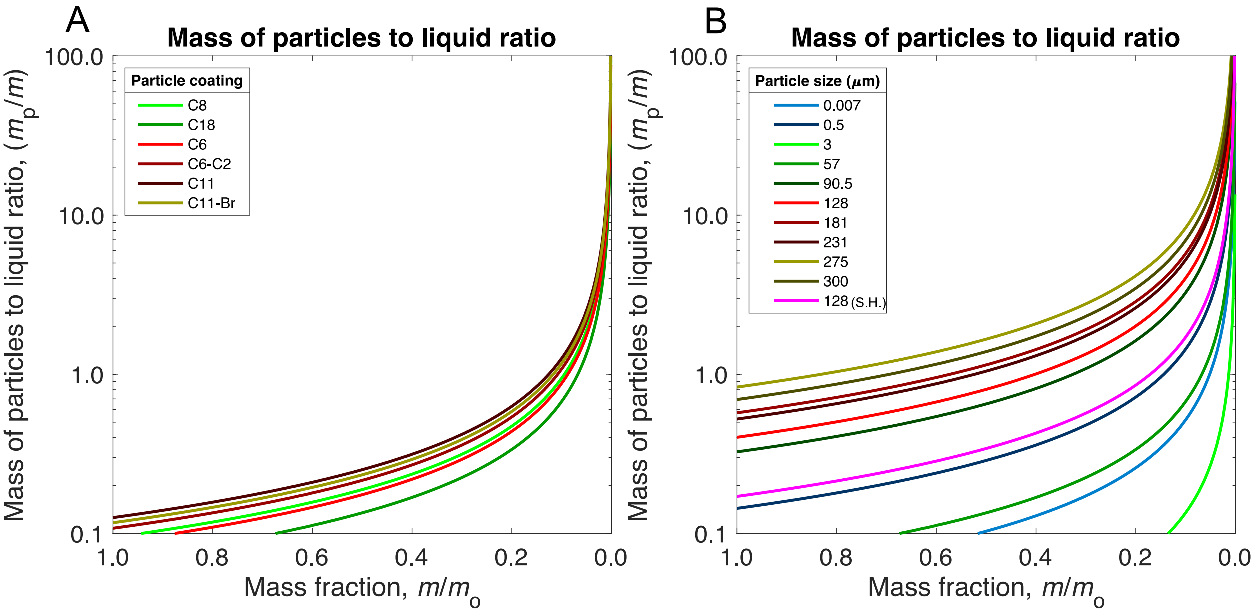

Fig. S9.

Ratio of mass of particles to the mass of liquid for 10-μL liquid marbles. (A) Different particle coatings at 57-μm particle size, and **(B)** different particle sizes with C18 coating.

Prediction of the apparent volume of liquid marbles

This study derived a formula for the characteristic diameter of liquid in the marble (see Eq. 9 in the manuscript). Accordingly, we can calculate the apparent volume of the liquid front, $V_{\mathrm{L,a}}$, approximated as a hemisphere (Eq. S2). This apparent volume of the liquid front (Eq. S1) differs from the actual volume of liquid (measured with a microbalance) because it represents the virtual volume of a hemispherical bare droplet, i.e., it has the same evaporation rate as a hemisphere of diameter D_{char}.

$$V_{\mathrm{L,a}} = \frac{2}{3}\pi\left(\frac{D_{\mathrm{char}}}{2}\right)^3 \tag{S1}$$

By adding the volume of dry particles, V_{P}, the apparent volume of the liquid marble, V_{M} (Eq. S2), is obtained. The volume of dry particles was experimentally determined through image analysis after complete evaporation of the liquid marbles, followed by logarithmic fitting against the surface particle density (Fig. S10).

$$V_M = V_{L,a} + V_P \tag{S2}$$

To obtain the experimental apparent volume of the liquid marble (Figs. S10B, D), we fitted the time-lapse images with a truncated ellipse of height, H_{M}, equatorial diameter, D_{M}, and base diameter, d, adjusted by the correct mass fractions, which were simultaneously recorded by a microbalance. Then, the apparent volumes were calculated through rotation around the central axis to form a truncated ellipsoid. However, note that a simple correlation (Eq. S3) for the measured height and largest diameter of the marble yielded accurate results with less than 3% deviation compared to the values obtained from the truncated ellipsoid. This approach generated greater errors when fitting Case I with smaller particle sizes ($\leq 57\ \mu m$) owing to its more deformed cup-like shape (Fig. 3B). The experimental D_{char} for the water droplet was calculated via volume fitting (Figs. S10A, C).

$$V_{\mathrm{M}} \approx \frac{3\pi}{16} H_{\mathrm{M}}.{D_{\mathrm{M}}}^2 \tag{S3}$$

Figure S10 shows that the modeled characteristic diameters and apparent volumes were greater than those of the water droplet or that of a reference perfect spherical (or hemispherical) droplet (denoted using the red dashed curve) in all cases but one. The exception was the 7-nm fumed silica marble (only negative k_{e}), which expectedly showed lower D_{char} owing to the increased resistance of vapor diffusion in the particle layer. In addition, evidently the experimental apparent volume of the liquid marble cannot be smaller than that of a spherical droplet; hence, the volume data points for the 7-nm silica marble do not fall below the diagonal curve except owing to fitting error. Notably, the bigger final volumes of the marbles of bigger particles clearly resulted from a higher particle to liquid volumetric fraction, as shown in Fig. S11. Furthermore, all D_{char} go to zero because it is the characteristic diameter of the liquid front, which does not consider the volume of particles.

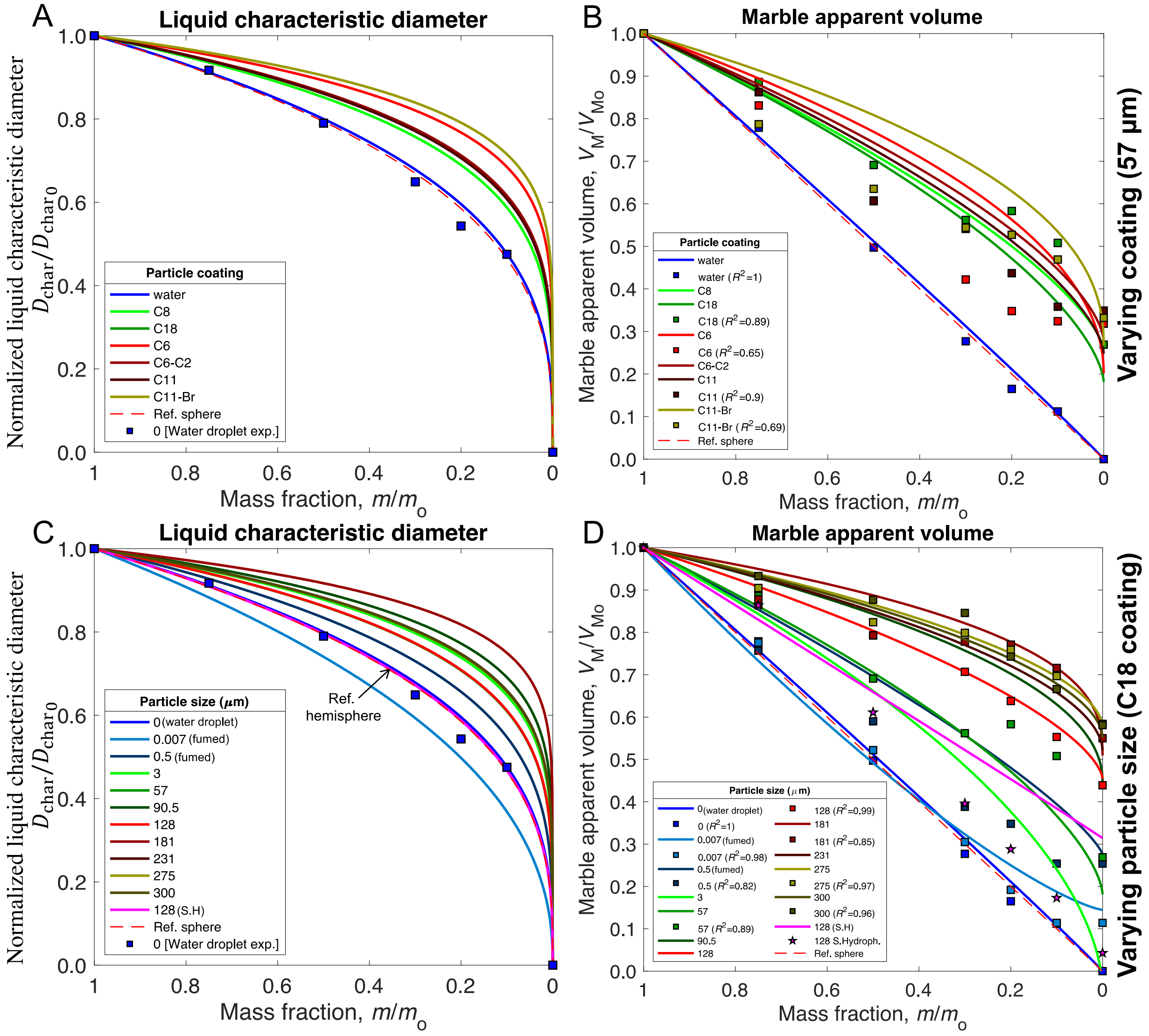

Fig. S10.

Prediction of marble characteristic dimensions. Experimental values are presented as points, and model predictions are depicted as lines. **(A, C)** Normalized liquid characteristic diameter and **(B, D)** normalized marble apparent volume compared to experimental results obtained from video analysis. **(A–B)** Varying particle coatings for 57-µm particle size. **(C, D)** Varying particle sizes for C18 coating (ODTS). Experimental data points for the marble apparent volume, V_M, are normalized by the initial marble apparent volume, V_{Mo}, fitted through image analysis of the evaporation time-lapse videos (Figs. 3 and S3).

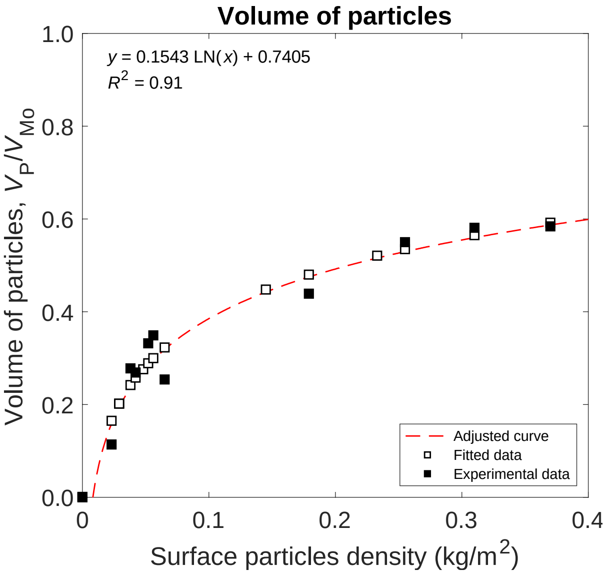

Fig. S11.

Dry volume of particles after complete evaporation. Volume of particles, V_P, relative to the initial volume of the liquid marble, V_{Mo}, as a function of the initial surface particle density for 10-µL water marbles.

Caption for Movie S1.

High-speed video of superhydrophobic sand grains (C18–128 µm) falling on a water droplet and forming a liquid marble.

Caption for Movie S2.

Time-lapse videos of the evaporation of liquid marbles formed from water droplets and particles whose characteristics are described below. (A) Water droplet on a hydrophobic glass slide (H-glass) and without particles (control case). **(B)** Case I for the evaporation of liquid marbles with hydrophobic particles of (Ba) 128 µm and (Bb) 57 µm size, maintaining a monolayer constant surface particle density and marble surface area together with low sphericity. **(C)** Case II for liquid marbles covered with superhydrophobic particles (128 µm) with particle ejection (for $m/m_o < 0.75$) and high liquid sphericity. **(D)** Case III for superhydrophobic fumed particles with increasing surface particle density caused by both increasing thickness and packing of particles at the liquid interface.